# Recirculation-enhanced switching in photonic crystal Mach-Zehnder interferometers

**T. P. White, C. Martijn de Sterke, R. C. McPhedran, and T. Huang**

*Centre for Ultrahigh-bandwidth Devices for Optical Systems (CUDOS) & School of Physics, University of Sydney, NSW 2006, Australia*

twhite@physics.usyd.edu.au

**L. C. Botten**

*Centre for Ultrahigh-bandwidth Devices for Optical Systems (CUDOS) & School of Mathematical Sciences, University of Technology, Sydney, NSW 2007, Australia*

**Abstract:** We show that Mach-Zehnder interferometers (MZIs) formed from waveguides in a perfectly reflecting cladding can display manifestly different transmission characteristics to conventional MZIs due to mode recirculation and resonant reflection. Understanding and exploiting this behavior, rather than avoiding it, may lead to improved performance of photonic crystal (PC) based MZIs, for which cladding radiation is forbidden for frequencies within a photonic bandgap. Mode recirculation in such devices can result in a significantly sharper switching response than in conventional interferometers. A simple and accurate analytic model is presented and we propose specific PC structures with both high and low refractive index backgrounds that display these properties.



**OCIS codes:** (130.3120) Integrated optics devices; (230.5750) Resonators; (050.2230) Fabry-Perot

## References and links

1. A. N. Chester, S. Martellucci, and A. M. V. Scheggi, eds., *Optical fiber sensors* (Martinus Nijhoff, Dordrecht, 1987).
2. G. V. Treyz, "Silicon Mach-Zehnder waveguide interferometers operating at 1.3 $\mu$m," Electron. Lett. **27**, 118–120 (1991).
3. C. Rolland, R. S. Moore, F. Shepherd, and G. Hillier, "10 Gbit/s, 1.56 $\mu$m Multiquantum well InP/InGaAsP Mach-Zehnder Optical Modulator," Electron. Lett. **29**, 471–472 (1993).
4. E. A. Camargo, H. M. H. Chong, and R. M. De. La. Rue, "Photonic crystal Mach-Zehnder structures for thermo-optic switching," Opt. Express **12**, 588–592 (2004). http://www.opticsexpress.org/abstract.cfm?URI=OPEX-12-4-588.
5. M. H. Shih, W. J. Kim, W. Kuang, J. R. Cao, H. Yukawa, S. J. Choi, J. D. O'Brien, and P. D. Dapkus, "Two-dimensional photonic crystal Mach-Zehnder interferometers," Appl. Phys. Lett. **84** (2004).
6. A. Martinez, A. Griol, P. Sanchis, and J. Marti, "Mach-Zehnder interferometer employing coupled-resonator optical waveguides," Opt. Lett. **28**, 405–407 (2003).
7. T. P. White, L. C. Botten, C. M. de Sterke, R. C. McPhedran, A. A. Asatryan, and T. N. Langtry, "Bloch mode scattering matrix methods for modelling extended photonic crystal structures. Part II: Applications," Phys. Rev. E (2004). To be published.
8. A. Lan, K. Kanamoto, T. Yang, A. Nishikawa, Y. Sugimoto, N. Ikeda, H. Nakamura, K. Asakawa, and H. Ishikawa, "Similar role of waveguide bends in photonic crystal circuits and disordered defects in coupled cavity waveguides: An intrinsic problem in realizing photonic crystal circuits," Phys. Rev. B **67** (2003).
9. T. P. White, L. C. Botten, R. C. McPhedran, and C. M. de Sterke, "Utracompact resonant filters in photonic crystals," Opt. Lett. **28**, 2452–2454 (2003).

#4517 - $15.00 US Received 2 June 2004; revised 21 June 2004; accepted 23 June 2004

10. L. C. Botten, T. P. White, A. A. Asatryan, T. N. Langtry, C. M. de Sterke, and R. C. McPhedran, "Bloch mode scattering matrix methods for modelling extended photonic crystal structures. Part I: Theory," Phys. Rev. E (2004). To be published.
11. L. C. Botten, T. P. White, C. M. de Sterke, R. C. McPhedran, A. A. Asatryan, and T. Langtry, "Photonic crystal devices modelled as grating stacks: matrix generalizations of thin film optics," Opt. Express **12**, 1592–1604 (2004). http://www.opticsexpress.org/abstract.cfm?URI=OPEX-12-8-1592.
12. G. P. Agrawal, *Fiber-optic communication systems*, 3rd ed. (John Wiley and Sons, New York, 2002).
13. M. Born and E. Wolf, *Principles of Optics*, 5th ed. (Pergamon, Oxford, 1975).
14. R. Wilson, T. J. Karle, I. Moerman, and T. F. Krauss, "Efficient photonic crystal Y-junctions," J. Opt. A **5**, S76–S80 (2003).
15. M. Tokushima, H. Yamada, and Y. Arakawa, "1.5 – $\mu$m-wavelength light guiding in waveguides in square-lattice-of-rod photonic crystal slab," Appl. Phys. Lett. **84**, 4298–4300 (2004).
16. Y. Sugimoto, Y. Tanaka, N. Ikeda, T. Yang, H. Nakamura, K. Asakawa, K. Inoue, T. Maruyama, K. Miyashita, K. Ishida, and Y. Watanabe, "Design, fabrication, and characterization of coupling-strength-controlled directional coupler based on two-dimensional photonic-crystal slab waveguides," Appl. Phys. Lett. **83**, 3236–3238 (2003).
17. A. Chutinan, S. John, and O. Toader, "Diffractionless flow of light in all-optical microchips," Phys. Rev. Lett. **90**, 123,901 (2003).
18. P. Lalanne, S. Mias, and J. P. Hugonin, "Two physical mechanisms for boosting the quality factor to cavity volume ratio of photonic crystal microcavities," Opt. Express **12**, 458–467 (2004). http://www.opticsexpress.org/abstract.cfm?URI=OPEX-12-3-458.

## 1. Introduction

Mach-Zehnder interferometers (MZIs) are used extensively in optical systems as filtering and switching devices and in phase measurement and detection applications. Their wide range of uses and functionality has led to the fabrication of MZI devices in fibers [1], planar dielectric waveguides [2], rib waveguides [3], and more recently two-dimensional photonic crystal (PC) waveguides [4, 5, 6]. Although the morphology of all MZIs is the same regardless of type of waveguide in which they are formed, the operational characteristics can be strongly influenced by the waveguide and cladding properties.

Conventional MZIs consist of waveguides that guide light due to total internal reflection. In these single-pass devices, light that is not transmitted into the output guide is radiated into the cladding and lost. However, if the cladding material is perfectly reflecting, radiation cannot occur and thus any light that is not transmitted must be reflected back into the interferometer. The resulting recirculating MZI can exhibit strong resonance effects that are not observed in conventional MZI devices. The observation of these effects relies critically on the use of beam splitters with very low reflectance ($< 2\%$). In Section 2 we present a simple modal analysis to analyze the transmission characteristics of recirculating MZIs and derive an elegant semi-analytic expression to describe their behavior. The properties of these devices are strikingly different from conventional MZIs, and our analysis shows that they are typical of a general class of MZI with perfectly reflecting cladding and single-mode input and output waveguides. One feature of these devices is an almost square transmission response with phase and thus a significantly sharper switching response than conventional MZIs. Such behavior is a highly desirable characteristic for both linear and nonlinear switching applications.

In Section 3 we propose two specific examples of recirculating MZIs using 2*D* photonic crystal waveguides with both high and low refractive index backgrounds. In both cases we use a novel junction type [7] that has the required low-reflectance properties. In this case, the perfectly reflecting cladding is provided by the photonic bandgap of the PC waveguide walls, which reflect light at all frequencies within the bandgap, regardless of incident angle. While it has been proposed that the strong reflections and associated interference observed in many PC based devices may limit their practical use in optical systems [8], these effects can also be used to great advantage. We recently proposed a novel PC-based filter that uses the strong reflection of waveguide modes to produce high-Q resonant transmission features [9], and a

#4517 - $15.00 US Received 2 June 2004; revised 21 June 2004; accepted 23 June 2004

similar approach was used to design the wide bandwidth Y-junctions [7] used here.

The PC MZI designs that we investigate in Section 3 are analyzed using rigorous 2*D* numerical calculations, and the results are compared to those of Section 2. As predicted by the model, the recirculating PC MZI designs exhibit highly unconventional properties that could provide novel response characteristics for future MZI devices.

## 2. Modal analysis of recirculating MZIs

We consider first the simple MZI illustrated in Fig. 1(a), consisting of single input and output waveguides, and two waveguide junctions $Y_1$ and $Y_2$ joined by waveguide arms $A_1$ and $A_2$ of length $L$. An ideal Y-junction splits light equally between $A_1$ and $A_2$. If an element is placed in $A_2$ to introduce a phase difference $\varphi$ between the two arms of the interferometer, the intensity of light transmitted into the output depends on $\varphi$. In a balanced MZI, $\varphi = 0$, so light entering from the input guide recombines in-phase at $Y_2$ and is transmitted into the output guide - a balanced MZI transmits equally well at all wavelengths. Active devices such as switches and filters can be made by varying $\varphi$ to modulate the output [4], or in passive devices, the output can be used to determine $\varphi$ [1].

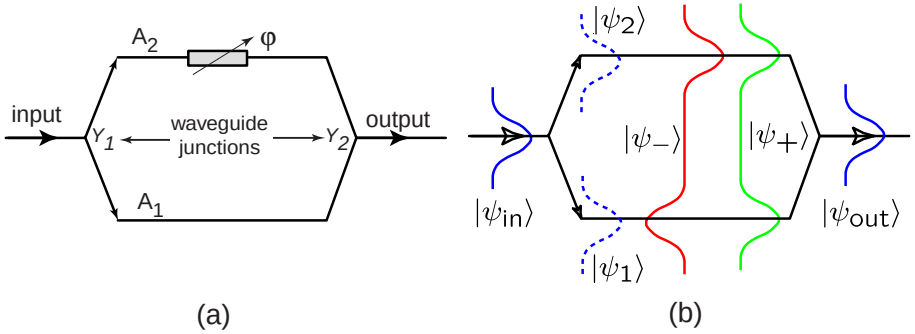


Fig. 1. (a) Schematic of a simple MZI with single input and output waveguides joined by arms $A_1$ and $A_2$ via Y-junctions $Y_1$ and $Y_2$. (b) Schematic of the propagating modes in each of the waveguide sections in (a). The green and red curves show the even and odd superpositions of the individual waveguide modes.

The transmission properties of the MZI in Fig. 1(a) are derived by considering the propagating modes in each of the waveguide sections. All waveguides are chosen to be identical, only supporting a single mode of even symmetry with respect to the waveguide axis. Thus, the input and output guides support one mode each, denoted by $|\psi_{\text{in}}\rangle$ and $|\psi_{\text{out}}\rangle$ respectively, and the two-guide region supports one mode in each of $A_1$ and $A_2$, denoted $|\psi_1\rangle$ and $|\psi_2\rangle$, as shown in Fig. 1(b). Alternatively, the modes in $A_1$ and $A_2$ are well approximated as a combination of two supermodes of even (+) and odd (-) symmetry with respect to the axis of the interferometer, indicated by the green and red curves in Fig. 1(b). The supermodes are approximately related to the modes in the individual guides by

$$|\psi_{\pm}\rangle = \frac{1}{\sqrt{2}}\left(|\psi_1\rangle \pm |\psi_2\rangle\right). \tag{1}$$

In an ideal structure, $A_1$ and $A_2$ are separated sufficiently that cross talk between the two guides is negligible, in which case the propagation constants of $|\psi_{\pm}\rangle$ are equal to the propagation constant of an isolated waveguide, $\beta_+ = \beta_- = \beta$ respectively. We return to this in Section 3.2.

Since mode $|\psi_{\text{in}}\rangle$ is symmetric with respect to $A_1$ and $A_2$, it can only couple to the supermode with the same symmetry, $|\psi_+\rangle$, so for an ideal $Y_1$ junction, mode $|\psi_{\text{in}}\rangle$ is fully transmitted

#4517 - $15.00 US
Received 2 June 2004; revised 21 June 2004; accepted 23 June 2004

into $|\psi_+\rangle$. When this mode propagates through $A_1$ and $A_2$, the effect of $\varphi$ is to introduce an asymmetric field component, equivalent to transferring some of the energy into $|\psi_-\rangle$. As at $Y_1$, the $|\psi_+\rangle$ component of the field entering $Y_2$ can couple into the output guide, but the $|\psi_-\rangle$ component cannot and must be either radiated or reflected.

To this point, the modal description holds for MZIs in general. The essential difference lies in what happens to $|\psi_-\rangle$ at $Y_2$. In dielectric waveguides, most of the light in $|\psi_-\rangle$ is radiated into the cladding and lost, and only a very small amount is reflected back into the arms of the interferometer. However, if light is unable to radiate into the cladding, any light in $|\psi_-\rangle$ must be reflected at $Y_2$, back into the interferometer. This odd mode reflection results in unique resonant behavior of recirculating MZIs with single-mode input and output waveguides.

We now follow the propagation of a mode $\Psi$ with unit energy $\langle\Psi|\Psi\rangle$ entering an unbalanced MZI from the input guide and consider the effect of odd mode reflection at $Y_2$. After passing through $Y_1$, the resulting field

$$|\Psi(0)\rangle^{(1)} = |\psi_+\rangle,$$

can be written in terms of $|\psi_1\rangle$ and $|\psi_2\rangle$ using Eq. (1). Here the superscript $(1)$ indicates that we are considering the fields on the first pass through the interferometer. The modes then propagate through each arm, essentially independently of each other, advancing in phase as they propagate. At $Y_2$, the combined field in $A_1$ and $A_2$ is

$$|\Psi(L)\rangle^{(1)} = \left(e^{i\beta L}|\psi_1\rangle + e^{i(\beta L+\varphi)}|\psi_2\rangle\right)/\sqrt{2} = e^{i\chi}\left(\cos(\varphi/2)|\psi_+\rangle - i\sin(\varphi/2)|\psi_-\rangle\right), \quad (2)$$

where $\chi = \beta L + \varphi/2$ and $\beta$ is the propagation constant of the single propagating mode of an isolated waveguide. At $Y_2$, the even field component is transmitted into the output guide, and the odd mode is reflected back into $A_1$ and $A_2$. Note that in a conventional MZI the odd mode is radiated into the cladding and the transmission is simply given by the even mode term in Eq. (2),

$$T = |e^{i\chi}\cos(\varphi/2)|^2 = \cos^2(\varphi/2) = \frac{1}{1+\tan^2(\varphi/2)}. \quad (3)$$

In the PC structure, however, the reflected odd field component, $-i\exp(i\chi)\sin(\varphi/2)|\psi_-\rangle$, propagates back through the two arms, accumulating a further phase $\varphi$ so that the field arriving back at $Y_1$ is

$$\begin{aligned} |\Psi(0)\rangle^{(2)} &= -ie^{i\chi}\sin(\varphi/2)\left(e^{i\beta L}|\psi_1\rangle - e^{i(\beta L+\varphi)}|\psi_2\rangle\right)/\sqrt{2} \\ &= -ie^{2i\chi}\sin(\varphi/2)\left(\cos(\varphi/2)|\psi_-\rangle - i\sin(\varphi/2)|\psi_+\rangle\right). \end{aligned} \quad (4)$$

Once again the odd field component is reflected back into the interferometer, while the even component is transmitted through the junction, in this case back into the input waveguide.

Repeating the above calculation for each pass of the odd mode through the interferometer, and summing the amplitudes of the fields transmitted into the output waveguide as a geometric series, we derive an expression for the overall transmitted intensity

$$T = \frac{4\sin^2(\chi)\cos^2(\varphi/2)/\sin^4(\varphi/2)}{1+4\sin^2(\chi)\cos^2(\varphi/2)/\sin^4(\varphi/2)}. \quad (5)$$

The reflected intensity ($R = 1-T$) can be derived in the same way by summing the field amplitudes transmitted from the interferometer back into the input waveguide. Observe that Eq. (5) is a function of both $\varphi$ and $L\beta = L\beta(\lambda)$, in contrast to the conventional MZI transmission (3), which is a function of $\varphi$ only. Thus, the dispersion properties of the waveguides are important in recirculating MZIs. Apart from the different functional forms of Eqs. (3) and (5), the additional

#4517 - $15.00 US Received 2 June 2004; revised 21 June 2004; accepted 23 June 2004

dependence on wavelength and structure length leads to significantly different transmission properties. The explicit dependence on structure length results from the mode recirculation inside the device. An alternative derivation of Eq. (5) for PC based MZIs follows directly from the rigorous Bloch mode method [10, 11] in the limit when we restrict the treatment to only include propagating modes and prescribe appropriate values for the various scattering matrices that accord with the above analysis.

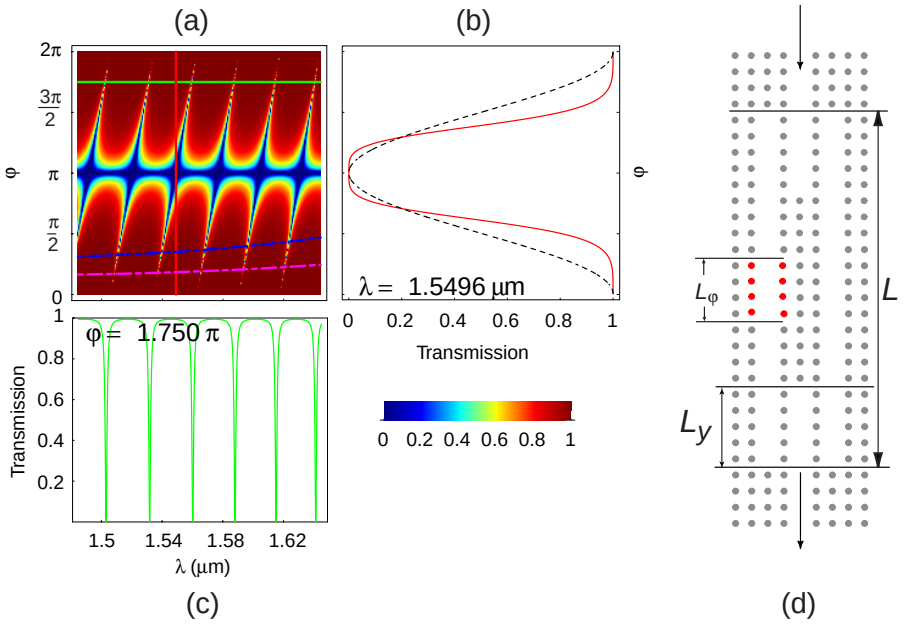


Fig. 2. (a) Transmission contour plot as a function of $\lambda$ and $\varphi$, calculated with Eq. (5) for a PC-based recirculating MZI with the geometry shown in (d), and parameters described in the text. The red and green lines correspond to the transmission plots in (b) and (c) at $\lambda = 1.5496\,\mu$m and $\varphi = 7\pi/4$, respectively. The dashed curve in (b) shows the transmission of a conventional MZI as a function of $\varphi$, given by Eq. (3). (d) Generic recirculating PC MZI formed in a square lattice of rods with the parameters given in the text. The red cylinders, with radius $a'$, are used to generate $\varphi$ in Section 3.1. The magenta and blue dashed-dotted curves in (a) show $\varphi$ as a function of $\lambda$ when $a' = 0.20d$ for $L_\varphi = 8d$ and $L_\varphi = 16d$ respectively. (Video file showing transmission as a function of $\lambda$ and $\varphi$ 1.9Mb)

Any calculation involving Eq. (5) requires numerical input of the wavelength variation of $\beta$, a property that depends on the geometry of the waveguides. In the remaining sections of this paper, the dispersion properties of photonic crystal waveguides are used in the numerical calculations, however the transmission behavior discussed is generic to all recirculating MZIs satisfying the conditions of the above analysis. This is exemplified in the two PC examples presented in Section 3; the waveguide dispersion properties are very different, with opposite dispersion slopes and strong dispersion near cutoff in one case, but the transmission characteristics bear a close resemblance to each other.

Figures 2(a)-(c) show the TM transmission of a recirculating MZI of length $L = 36d = 19.9\,\mu$m, calculated using Eq. (5). The wavelength dependence of $\beta$ was calculated for a single waveguide formed by removing one row of rods from the square PC lattice of period $d = 570\,$nm shown in Fig. 2(d). The PC consists of dielectric rods of radius $a = 0.18d$, and refractive index $n_{\rm cyl} = 3.4$, in a background of air ($n_b = 1$). Figure 2(a) is a contour plot of transmission as a

#4517 - $15.00 US
Received 2 June 2004; revised 21 June 2004; accepted 23 June 2004

function of wavelength and phase difference, where the red areas correspond to high transmission, and the blue areas correspond to low transmission (high reflection). The transmission is high across much of the parameter space, and in particular it can be seen that $T = 1$ when $\varphi = 0$ and $T = 0$ when $\varphi = \pi$, as for a conventional MZI. The slightly tilted, low transmission 'valleys' correspond to strong resonances due to the multiple reflections of the odd mode. At the center of the valleys, the transmission drops to zero and the valleys become rapidly narrower as $\varphi$ approaches 0 or $2\pi$. The slight tilt of the valleys from vertical is determined by the dispersion slope of $\beta$, which appears in $\chi$ in Eq. (5).

We first consider the properties of Eq. (5) as $\varphi$ is varied at a fixed wavelength, corresponding to traversing a vertical line across Fig. 2(a). For most wavelengths, a vertical line intersects one end of a low transmission valley, resulting in a transmission response with a strong resonant reflection, the width decreasing as the resonance position approaches $\varphi = 0$ or $\varphi = 2\pi$. There are, however, wavelengths for which the sharp resonances are avoided. Of particular interest is the response of the MZI at the wavelengths where the diagonal valleys intersect the low transmission band at $\varphi = \pi$. The red curve in Fig. 2(b) shows the response as a function of $\varphi$ at one of these wavelengths, $\lambda = 1.5496\,\mu$m, corresponding to the red line in Fig. 2(a). The dashed curve on the same axes shows the transmission of a conventional MZI, given by Eq. (3). Comparing the two curves, it is seen that the recirculating MZI response exhibits a significantly sharper transition between 'on' and 'off' states. From Eq. (5), we find that this behavior occurs when $\beta L = \pi/2, 3\pi/2, 5\pi/2\ldots$, for which

$$T = \frac{4\cot^4(\varphi/2)}{1+4\cot^4(\varphi/2)} = \frac{1}{1+\tan^4(\varphi/2)/4}. \tag{6}$$

Note that although the specific waveguide geometry determines the wavelengths at which this condition occurs, when it is satisfied, the phase response is entirely independent of the waveguide properties.

Comparing Eqs. (3) and (6), we see that the recirculating MZI response is quartic in $\tan(\varphi/2)$, compared with the quadratic response of a conventional MZI. The change in $\varphi$ required to switch the transmission from 0.9 to 0.1 in the recirculating MZI is approximately $0.32\pi$, whereas a conventional MZI would require a change of $0.59\pi$. Although $\cos^4(\varphi/2)$ responses can be achieved with a pair of conventional MZIs, and higher order behavior occurs for a chain of such devices [12], we find that at least 6 identical conventional MZIs would be required to obtain a superior switching performance to that of a single recirculating MZI. Note, also, that the transmission given by Eq. (6) has a fourth-order variation near both $T = 0$ and $T = 1$, whereas a chain of MZIs always shows a quadratic variation in the region around $T = 1$. The steep, almost square response exhibited by the recirculating MZI is highly desirable for switching applications, and could be used to improve performance in both linear and nonlinear devices.

If the wavelength is varied while $\varphi$ is fixed, the transmission properties are very different from the examples of Fig. 2(b). In this case, $T$ is a function of $L\beta(\lambda)$, and Eq. (5) closely resembles the expression for the reflectance of a Fabry-Perot etalon [13] with finesse

$$\mathscr{F} = \frac{\pi|\cos(\varphi/2)|}{1-|\cos(\varphi/2)|}. \tag{7}$$

Thus, the transmission behavior of the recirculating MZI is essentially the reverse of a Fabry-Perot etalon, exhibiting resonant reflection, rather than resonant transmission. This is seen in Fig. 2(a), where horizontal lines of constant $\varphi$ intersect the reflection resonances. As $\varphi$ approaches 0 or $2\pi$, these bands become narrower, and the finesse increases according to Eq. (7). Fig. 2(c) shows the transmission as a function of $\lambda$ when $\varphi = 7\pi/4$, for which the finesse given

#4517 - $15.00 US Received 2 June 2004; revised 21 June 2004; accepted 23 June 2004

by Eq. (7) is $\mathscr{F} = 38$ and the fringe visibility is very close to 1. As $\varphi$ approaches $\pi$, both the fringe visibility and the finesse decrease. These reversed Fabry-Perot transmission characteristics could be used in the design of a tunable notch rejection filter where the finesse and resonance position could be adjusted by varying $\beta$ and $\varphi$.

In practice, $\varphi$ is a function of wavelength, and so it would be difficult to design a device to exhibit the transmission spectra shown in Fig. 2(c). Any realistic measurement of transmission spectra would correspond to the transmission along a curved line in Fig. 2(a), the exact shape of such a curve being determined by the method used to induce $\varphi$. This aspect is discussed further in Sections 3.1 and 3.2 below.

## 3. Photonic crystal recirculating MZI structures

In the previous section, we derived a simple model for the transmission of an ideal MZI with a perfectly reflecting cladding and single-mode input and output guides, and showed that recirculation and resonant properties occur due to the reflection of modes with odd symmetry at the waveguide junctions. In this section we present rigorous numerical calculations of two specific PC MZI designs that display these characteristics and compare them to the semianalytic results of Eq. (5). Recall that the Y-junctions in the model were taken to be ideal, transmitting modes of even symmetry and reflecting modes of odd symmetry. In practice, the even mode is not perfectly transmitted, and the additional reflected fields can result in additional strong Fabry-Perot resonances [4] that mask the odd mode effects. From our numerical studies, we find that the odd mode effects are most clearly observed when the even mode transmission exceeds 98%. Thus, to observe the properties predicted by Eq. (5), the junction design is critical. We recently proposed a novel PC coupled Y-junction design that exhibits very high transmission over wide bandwidths [7] due to a combination of directional coupling and mode recirculation behavior. Figure 3(a) shows the coupled Y-junction used in the PC MZI studied in Section 3.2. The transmission of this junction is plotted in Fig. 3(b), showing the 98% bandwidth of approximately 36 nm - considerably broader than many of the PC Y-junction designs reported to date [5, 14]. The junction used for the PC MZI in Section 3.1 is similar in design, but formed in a PC with high-index rods in a low-index background. Both junctions are ideal for use in recirculating PC MZI designs as we demonstrate in the following examples.

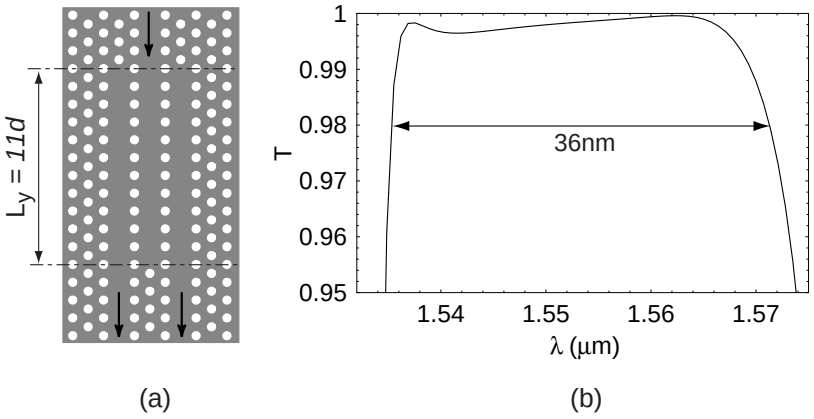


Fig. 3. (a) Y-junction used in the PC MZI design of Section 3.2. (b) Transmission through the junction as a function of wavelength. The 98% transmission bandwidth is approximately 36 nm.

#4517 - $15.00 US
Received 2 June 2004; revised 21 June 2004; accepted 23 June 2004

### 3.1. *Dielectric rod square lattice PC MZI*

The MZI design shown in Fig. 2(d) is formed in the square lattice of dielectric cylinders with the parameters described in Section 2. This PC lattice exhibits a bandgap for TM polarized light in the wavelength range $2.249d \leq \lambda \leq 3.306d$. A waveguide formed by removing a single line of cylinders supports a single propagating mode of even symmetry in the wavelength range $2.249d \leq \lambda \leq 3.205d$. Experimental results for similar dielectric rod PC waveguide structures have recently been reported [15].

The coupled Y-junction shown in Fig. 2(d) has a 98% transmission bandwidth of about 150 nm at $\lambda = 1.55\,\mu$m, that roughly defines the operating bandwidth of the MZI. We generate $\varphi$ by changing the radii of $L_\varphi/d$ pairs of cylinders on either side of one waveguide from $a$ to $a'$ as indicated by the red cylinders in Fig. 2(d). This changes the modal propagation constant of that section of waveguide by $\Delta\beta \ll \beta$, introducing a total phase difference of $\varphi = \Delta\beta L_\varphi$. The change in radius is chosen to be small enough that there is no significant reflection produced by the change in the guide properties. We choose this approach for illustrative purposes only, as it is a convenient way of generating $\varphi$ for our numerical formulation, which is based on a Bloch mode scattering matrix method [10, 11]. In practice, $\varphi$ could be varied by using, for instance, localized heating, as in Ref. [4] to change the propagation properties of one waveguide arm.

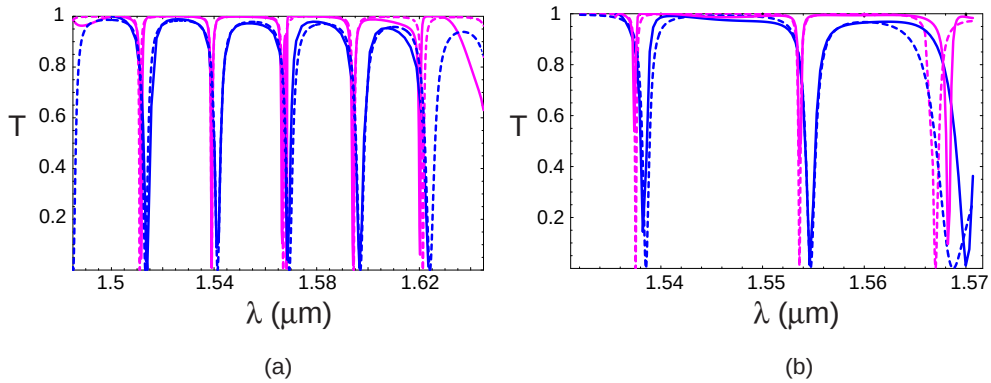


Fig. 4. Comparison of the transmission of the PC MZIs calculated with the rigorous numerical calculations (solid curves) and the semianalytic results of Eq. (5) (dashed curves). (a) TM transmission of the PC MZI shown in Fig. 2(d) with $L = 36d$, $L_y = 5d$, $a' = 0.20d$ and $L_\varphi = 8d$ (magenta) and $L_\varphi = 16d$ (blue). (b) TE transmission of the PC MZI shown in Fig. 5(d) with $L = 37d$, $L_y = 11d$, $a' = 0.30d$ and $L_\varphi = 3d$ (magenta) and $L_\varphi = 7d$ (blue).

Since $\beta$ and hence $\Delta\beta$ are functions of wavelength, $\varphi$ is also wavelength dependent in this example. Figure 4(a) shows the transmission of two MZIs with $L_\varphi = 8d$ and $L_\varphi = 16d$ respectively for $a' = 0.2d$ and $L = 36d$. The solid curves are calculated using the full Bloch mode numerical calculation, and the dotted curves are the result of Eq. (5), calculated along the dashed-dotted curves in Fig. 2(b) to account for the wavelength dependence of $\varphi$. As expected from Eq. (7), the resonances are considerably narrower for the $L_\varphi = 8d$ structure, since $\varphi \approx L_\varphi \Delta\beta$. The parameters $L$ and $L_\varphi$ used in Eq. (5) are not necessarily identical to those used to define the structure in Fig. 2(d). Since PCs behave as distributed reflectors, defining a structure length is somewhat ambiguous. We find that the best agreement in resonance position occurs when we take $L$ in Eq. (5) to be the total length of the structure, including the junctions, as shown in Fig. 2(d), with a slight correction for the phase change introduced by reflection from the PC. Under these conditions, the agreement between the rigorous numerical result, and the semi-analytic model is excellent. In particular, the model predicts the resonance widths with

#4517 - $15.00 US
Received 2 June 2004; revised 21 June 2004; accepted 23 June 2004

very good accuracy, and with the adjusted parameter $L$, the resonance positions are also closely matched.

### 3.2. *Air hole triangular lattice PC MZI*

We briefly present a PC MZI design in a triangular PC lattice of air holes ($n_{\mathrm{cyl}} = 1$) with period $d = 350\,\mathrm{nm}$ and radius $a = 0.32d$ in a dielectric of refractive index $n_b = 3.4$. An infinite lattice with these parameters exhibits a TE bandgap between $3.506d \leq \lambda \leq 3.761d$. In contrast to the dielectric rod PC in the previous example, $W1$ waveguides formed in triangular lattices of air holes typically support more than one mode at some frequencies in the bandgap. Since the odd-mode resonance properties rely on the input and output guides being single-mode, the structure shown in Fig. 5(d) is designed to operate in the low-frequency region of the bandgap where a single mode is supported for $4.100d \leq \lambda \leq 4.515d$. The mode has strong dispersion as it approaches cutoff near the low frequency end of this range which causes the MZI transmission properties to vary with wavelength more than the example in Section 3.1.

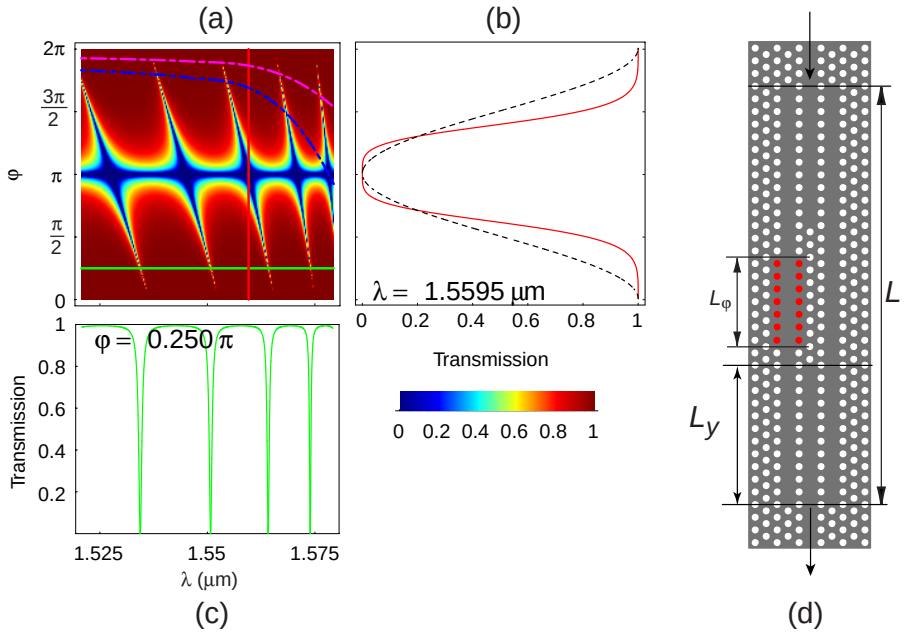


Fig. 5. (a) Transmission contour plot calculated with Eq. (5) for a PC MZI with the geometry shown in (d), and parameters described in the text. The red and green lines correspond to the transmission plots in (b) and (c) at $\lambda = 1.5595\,\mu\mathrm{m}$ and $\varphi = \pi/4$, respectively. The dashed curve in (b) is the response of a conventional MZI, as given by Eq. (3). (d) Generic PC MZI formed in a triangular lattice of air holes with the parameters described in the text. The red cylinders, with radius $a'$ are used to generate $\varphi$. The magenta and blue dashed-dotted curves in (a) show $\varphi$ as a function of $\lambda$ when $a' = 0.30d$ for $L_\varphi = 3d$ and $L_\varphi = 7d$ respectively. (Video file showing transmission as a function of $\lambda$ and $\varphi$ 1.9Mb)

Figure 5(d) shows the MZI design in the air hole triangular lattice. The optimum coupled Y-junction in this PC has a length $L_y = 11d$, as shown in Fig. 3. As in Section 3.1, the radii of $L_\varphi/d$ pairs of cylinders are varied in order to generate $\varphi$, as indicated by the red cylinders in Fig. 5(d). Figure 5(a) is a contour plot of the transmission for an MZI of this type, calculated as a function of wavelength and $\varphi$ using Eq. 5. In comparing Eq. (5) with full numerical calculations of the realistic structure (Fig. 4(b)), we have found that the agreement is improved

#4517 - $15.00 US
Received 2 June 2004; revised 21 June 2004; accepted 23 June 2004

at longer wavelengths if $\beta$ is replaced with $\beta_-$ in the model. This slight modification makes sense since the resonances are driven by multiple reflections of the odd mode. In the example of Section 3.1, $\beta$ and $\beta_-$ were essentially equal, so such a modification makes little difference to the comparison in Fig. 4(a).

There are some clear differences between the contour plots in Figs. 5(a) and 2(a). First, the low transmission valleys run in the opposite diagonal direction because of the different dispersion slopes of the waveguide modes in the two PC structures. Second, in Figs. 5(a) the tilt and the separation of the resonances changes significantly at longer wavelengths, whereas in Fig. 2(a), the valleys remain almost parallel and equally spaced. This is also a result of the different dispersion curves. The modes of the MZI in Fig. 2(d) are well away from cutoff, so the dispersion slope is relatively constant, resulting in the regular appearance of Fig. 2(a). In contrast, the modes of the MZI in Fig. 5(d) are closer to cutoff and the resulting strong dispersion distorts the transmission profile. This is also seen in Fig. 5(c) where the transmission is plotted as a function of wavelength for fixed $\varphi = \pi/2$. The spacing of the resonances decreases with increasing wavelength, while the resonances become narrower, maintaining a constant finesse.

Despite the differences in the transmission properties of the two examples here, the quartic response with $\varphi$, given by Eq. (6), is unchanged, as shown by the example in Fig. 5(c), where the transmission is plotted as a function of $\varphi$ for $\lambda = 1.5595\,\mu$m, indicated by the red line in Fig. 5(a).

Figure 4(b) shows the transmission as a function of wavelength for two MZIs of the type shown in Fig. 5(d) with $L_\varphi = 3d$ and $L_\varphi = 5d$ respectively for $a' = 0.30d$ and $L = 37d$. The solid curves are the full numerical result, and the dotted curves are given by Eq. (5), calculated along the magenta ($L = 3d$) and blue ($L = 7d$) curves shown in Fig. 5(a), corresponding to the wavelength variation of $\varphi = \Delta\beta L$. Once again we see that the semianalytic model predicts accurately the finesse of the resonances. The resonance positions line up very closely at the shorter wavelength end of the transmission region, however the agreement is poorer at longer wavelengths, again due to the strong modal dispersion close to cutoff.

## 4. Discussion and conclusion

We have shown that MZIs formed from waveguides with a perfectly reflecting cladding display significantly different transmission characteristics to conventional MZIs. In particular, reflections due to modal symmetry mismatches result in mode recirculation and resonant transmission behavior. Photonic crystals provide one means of obtaining a reflecting cladding with the required properties to demonstrate such behavior.

Examples of specific device designs exhibiting these characteristics have been presented for 2*D* PCs with both high index inclusions in a low index background, and the inverted geometry. We note that alternative junction designs based on directional couplers [16] with two input and output ports would not display these properties, since modes of both odd and even symmetry can be transmitted through such junctions. Although we have not explicitly studied the radiation losses of such devices, as with any cavity within a 2*D* PC, the out-of-plane losses must be considered and minimized to achieve a practical device. One way of achieving this would be to incorporate a 3*D* PC layer above and below the waveguide layer, as proposed in [17]. Alternatively, radiation losses could be reduced by tuning the cavities to minimize coupling into radiation modes above and below the waveguides [18].

The semi-analytic model derived in Section 2 gives insight into the physics of MZIs and provides a powerful design tool for rapidly predicting the properties of relatively complicated devices knowing only the dispersion properties of a single waveguide. An example of this was given in Section 2 where we derived the requirements for a recirculating MZI with a transmission response that has a quartic phase dependence, and a correspondingly steep response

#4517 - $15.00 US Received 2 June 2004; revised 21 June 2004; accepted 23 June 2004

curve linking a flat high transmission region to a flat low transmission region. A device with such a response could provide enhanced switching performance in both linear and nonlinear applications.

**Acknowledgments**

This work was produced with the assistance of the Australian Research Council under its ARC Centres of Excellence Program.

#4517 - $15.00 US Received 2 June 2004; revised 21 June 2004; accepted 23 June 2004